





# Optical, structural, and functional properties of highly reflective and stable iridium mirror coatings for infrared applications

PAUL SCHMITT,<sup>1,2</sup>  NADJA FELDE,<sup>1</sup> THORSTEN DÖHRING,<sup>3</sup>  
MANFRED STOLLENWERK,<sup>3</sup> INGO USCHMANN,<sup>4</sup> KEVIN HANEMANN,<sup>1</sup>  
MARIE SIEGLER,<sup>1</sup> GEORG KLEMM,<sup>1</sup> NANCY GRATZKE,<sup>1</sup> ANDREAS  
TÜNNERMANN,<sup>1,2</sup> STEFAN SCHWINDE,<sup>1</sup> SVEN SCHRÖDER,<sup>1</sup> AND  
ADRIANA SZEGHALMI<sup>1,2,\*</sup> 

<sup>1</sup>Fraunhofer Institute for Applied Optics and Precision Engineering IOF, Center of Excellence in Photonics, Albert-Einstein-Str. 7, D-07745 Jena, Germany

<sup>2</sup>Friedrich Schiller University Jena, Faculty of Physics and Astronomy, Institute of Applied Physics IAP, Albert-Einstein-Str. 15, D-07745 Jena, Germany

<sup>3</sup>TH Aschaffenburg - University of Applied Sciences, Würzburger Str. 45, D-63743 Aschaffenburg, Germany

<sup>4</sup>Friedrich Schiller University Jena, Faculty of Physics and Astronomy, Institute of Optics and Quantum Electronics IOQ, Max-Wien-Platz 1, D-07743 Jena, Germany

\*a.szeghalmi@uni-jena.de

**Abstract:** Metallic coatings are essential for numerous optical systems due to their high and broadband reflectivity in the infrared spectral range. In contrast to well-established (protected) silver and gold mirror coatings, iridium is environmentally durable, referring to ISO 9211-3 and thermally stable up to 600 °C even without protective layers, as demonstrated. Additionally, the optical and related structural properties of atomic layer deposited (ALD) and magnetron sputtered (MS) Ir coatings were investigated using spectrophotometry, FTIR, ellipsometry, WLI, AFM, XRR, XRD, SEM, and electrical resistivity measurements. The properties of Ir ALD and Ir MS coatings differ due to their topography and microstructure.

© 2022 Optica Publishing Group under the terms of the [Optica Open Access Publishing Agreement](#)

## 1. Introduction

Metallic functional coatings are essential for numerous optical elements in spectroscopy, sensing, lighting, and astronomy [1–3]. The well-established mirror coatings of silver (Ag) and gold (Au) provide a high and broadband intrinsic reflectivity in the infrared (IR) spectral range for such applications. However, without suitable protective layers, these metallic coatings are susceptible to environmental influences and mechanical stress, which decreases their reflectance significantly. In contrast, the noble metal iridium (Ir) exhibits a high reflectivity comparable to Ag and Au coatings in the mid-infrared (MIR) spectral range and high resistance to environmental influences even without protective layers, as demonstrated in this article.

The absence of protective layers offers several advantages. For example, to protect the surface of sensitive metal mirrors or enhance their reflectance [4], metal oxide layers (e.g., SiO<sub>x</sub> and Al<sub>2</sub>O<sub>3</sub> [5–7]), nitrides (e.g., SiN<sub>x</sub> [7,8]), oxynitrides (e.g., AlO<sub>x</sub>N<sub>y</sub> [9]), and laminates [10,11] are usually applied. However, such dielectric coatings exhibit absorption bands in the IR spectral range due to vibrational modes reducing the achievable reflectivity [12,13]. Furthermore, the in-situ preparation of metal oxide or nitride layers in the same deposition chamber impairs the high-purity metallic coatings. In contrast, Ir mirrors do not require protective layers due to their high intrinsic stability [14,15]. Thus, the associated deposition steps and optimization for protective layers are obsolete. In addition, high-quality Ir coatings can be deposited conformally on complex shaped or nanostructured substrates using atomic layer deposition (ALD) [16].

Iridium coatings are not applied as mirrors for the IR spectral range yet. In optics, Ir coatings are mainly applied for the X-ray regime and ultraviolet (UV) to visible (VIS) spectral range, such as Fresnel zone plates [17], mirrors [18–22], and metal wire grid polarizers [23]. Further applications include sensors [24], catalysts [25–27], electrodes [28,29], protective layers [30], and hydrogen separation membranes [31]. However, this work demonstrates the application potential of Ir mirror coatings for the IR spectral range and compares their performance to protected Ag and Au mirrors.

This article presents highly reflective and stable Ir coatings as mirrors for the MIR spectral range. Therefore, unprotected Ir coatings were prepared by ALD and magnetron sputtering (MS) and compared to commercially available protected Ag (stock number #36-043) and Au (#43-733) mirror coatings from Edmund Optics (UK). Without protective layers, the Ir coatings are environmentally durable and thermally stable, ensuring constant reflectance from 200 nm to 20  $\mu\text{m}$  wavelength. Certainly, Ir coatings cannot replace the established mirror materials but may serve as a reasonable alternative in particular cases and extend the usable material portfolio for optical coatings.

The results of this article are divided into two parts. The first part presents the optical and related structural properties of Ir coatings fabricated by ALD and MS. Spectrophotometry (SP), Fourier-transform infrared spectroscopy (FTIR), variable-angle spectroscopic ellipsometry (SE), white light interferometry (WLI), and atomic force microscopy (AFM), as well as X-ray reflectometry (XRR), X-ray diffraction (XRD), scanning electron microscopy (SEM), and four-point probe resistivity measurements were applied for this detailed material characterization. In the second part, the functional properties, namely the environmental durability referring to ISO 9211-3 and thermal stability up to 600  $^{\circ}\text{C}$  regarding their reflectance, were investigated and compared to the protected Ag and Au coatings. Additionally, top-view microscopy images of the mirror coatings were obtained.

## 2. Materials and methods

As substrate materials, silicon (Si) wafers with a 1 - 2 nm thick native  $\text{SiO}_2$  top layer and fused silica (FS) were used. The Si wafers were single-crystalline, (100)-orientated, p-doped, double side polished with an AFM ( $1 \times 1 \mu\text{m}^2$ ) surface roughness of about 0.15 nm root-mean-square (rms), and  $25 \times 25 \times 0.675 \text{ mm}^3$  in size. The amorphous FS substrates had an AFM surface roughness of about 0.26 nm rms, 25 mm diameter, and 1.0 mm thickness. For cleaning, a multi-stage, ultrasonic-assisted bath cleaning system (Elma Schmidbauer, Germany) was used with surfactants and water ( $\text{H}_2\text{O}$ ) baths, concluded by a deionized (DI), ultra-pure  $\text{H}_2\text{O}$  bath.

The poly-crystalline iridium coatings were fabricated by atomic layer deposition (ALD) and magnetron sputtering (MS) on Si wafers and FS. For the ALD depositions, a commercial ALD system SunALE R-200 Advanced (Picosun Oy, Finland) as well as iridium(III) acetylacetonate ( $\text{Ir}(\text{acac})_3$ ) and molecular oxygen ( $\text{O}_2$ , purity level 4.5) as precursors were used, as previously reported [32,33]. The MS depositions were performed with a radio frequency (RF) magnetron sputtering machine VPA 21 (Aurion Anlagentechnik, Germany) using a pure Ir target (purity level 3N = 99.9%) and argon (Ar, purity level 5.0) as the sputtering gas. As already known, the structure of sputtered metallic coatings strongly depends on the sputter parameters [34]. In order to achieve smooth and dense Ir layers, an RF sputtering power of 300 W and actively controlled process pressure of about 0.5 Pa were used, as demonstrated in previous studies [35,36]. For optically dense Ir coatings, an Ir layer thickness of 60 - 80 nm was targeted. Buffer layers of about 10 nm  $\text{Al}_2\text{O}_3$  [32] and 50 nm Cr [19,37] for the ALD and MS deposited Ir coatings, respectively, ensure adhesion to the substrate. After deposition and exposure to air, the Ir coatings were stored under ambient conditions at room temperatures (RT) of  $(23 \pm 5) ^{\circ}\text{C}$  and  $(45 \pm 20) \%$  relative humidity (RH).

Reflectance and optical constants were determined using SP, FTIR, and SE. The reflectance was measured with a two-beam spectrophotometer Lambda 900 (PerkinElmer, MA, USA) at 6° angle of incidence from 200 nm to 2500 nm wavelength, a two-beam spectrophotometer Cary 7000 UMS (Agilent Technologies, CA, USA) at 15°, 30°, 45°, and 60° angle of incidence in s- and p-polarization from 400 nm to 2500 nm, and an FTIR spectrometer Frontier Optica (Perkin Elmer) in reflection mode at 10° angle of incidence from 2400 nm to 20  $\mu\text{m}$ . The measurement uncertainties vary from about 0.25% (UV) to 0.15% (VIS to near IR) and 0.2% (MIR < 10  $\mu\text{m}$ ), 0.5% (< 15  $\mu\text{m}$ ), and 1.0% (< 20  $\mu\text{m}$ ). In addition, the ellipsometric parameters  $\Psi$  and  $\Delta$  were determined with a spectroscopic ellipsometer SE850 DUV (Sentech Instruments, Germany) at angles of incidence between 40° and 70° in 5° steps from 190 nm to 980 nm wavelength. By combining these consistent measurements, the optical constants of Ir were evaluated using the software package SpetraRay/4 (Sentech Instruments).

WLI and AFM were applied to characterize the topography of the Ir coatings. For the WLI measurements, a NewView 7300 (Zygo, CT, USA) system with magnifications of 10x and 50x was used. AFM measurements were performed using a Dimension Icon system (Bruker, MA, USA) and single-crystalline Si probes with a nominal tip radius of 5 nm. Samples areas of  $1 \times 1 \mu\text{m}^2$ ,  $10 \times 10 \mu\text{m}^2$ , and  $50 \times 50 \mu\text{m}^2$  were scanned in tapping mode. For each WLI and AFM measurement area, the power spectral density (PSD) function was calculated, characterizing the relative strength of each roughness component in terms of spatial frequencies. These single PSD functions were combined by geometrically averaging to the so-called Master-PSD function [38].

Additionally, structural Ir properties were analyzed using XRR, XRD, SEM, and four-point probe resistivity measurements. For XRR and XRD, a D8 Discover (Bruker AXS, Germany) diffractometer in Bragg-Brentano geometry with Cu  $K\alpha$  radiation ( $\lambda = 0.154 \text{ nm}$ ), 40 kV acceleration voltage, and 40 mA cathode current was used. The XRR data were fitted using the software package Leptos 7 (Bruker AXS). The Ir crystallite sizes within the Ir layer were estimated using the Ir(111) diffraction peak and Scherrer's equation with a shape factor of  $K \approx 0.94$  [39]. For SEM analysis, a Schottky field emission SEM ZEISS Sigma (Carl Zeiss Microscopy, Germany) with 5 kV acceleration voltage, 4.9 mm working distance, and an in-lens detector providing a resolution of about 2 nm was used. The four-point probe resistivity measurements were performed with digital multimeters Keithley 2601 (Keithley Instruments, OH, USA) and Keithley 2000. The contact tips with a distance of 2.54 mm were placed in the sample middle using a correction factor of  $G = 4.344$  [40] for calculations.

The unprotected Ir and protected Ag and Au mirror coatings were tested concerning environmental durability and thermal stability. Their environmental durability was tested referring to ISO 9211-3 and related testing standards [41]. For adhesive strength tests, a high tear-resistant, transparent tape of polyester 3M 853 TAPE (3M, MN, USA) was used. Climate tests were performed with a climate cabinet MKFT 240 (Binder, Germany). Thermal stability was evaluated using a custom-made vacuum (pressure <  $5.0 \cdot 10^{-5} \text{ Pa}$ ) tempering furnace (Systec Fertigungstechnik, Germany). The samples were heated at 10 K/min, held at the target temperature for 24 h, and passively cooled to 60 °C maximum. After each test, the samples were inspected by the unaided eye and optionally with a Leica DM6000 microscope (Leica Camera, Germany) with 10x magnification and Zeiss Axiocam (Carl Zeiss Microscopy, Germany).

### 3. Results and discussion

#### 3.1. Optical and structural properties of iridium coatings

The reflectance of iridium coatings in the IR spectral range is comparable to currently established mirror coatings. Figure 1(a) shows the reflectance of unprotected Ir coatings fabricated by ALD and MS compared to commercially available protected Ag and Au mirror coatings from 200 nm to 20  $\mu\text{m}$  wavelength. For wavelengths  $\gtrsim 3 \mu\text{m}$ , the Ir reflectance becomes similar to that of the protected Ag and Au coatings, as the inset illustrates. Indeed, Ag and Au have partially higher

reflectance than Ir, but some absorption bands (mainly around 2.9  $\mu\text{m}$  and 9.5  $\mu\text{m}$ ) reduce their reflectance significantly. These absorption bands and the oscillations in the UV-VIS spectral range originate from the protective layers (the supplier has not disclosed their composition). The results for Ir coatings deposited on Si wafers and FS were identical within the measurement accuracy. Unless otherwise stated, all results for Ir refer to Si wafers as substrate material. However, Fig. 1(a) shows some reflectance differences between the ALD and MS deposited Ir coatings.

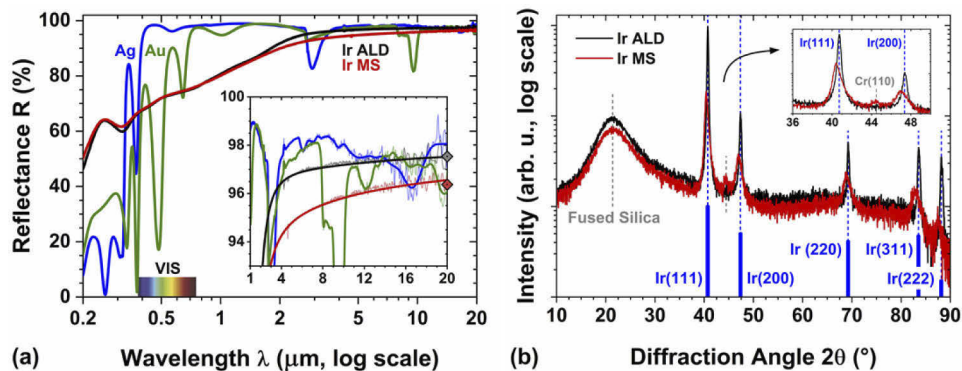


**Fig. 1.** (a) Specular reflectance of unprotected iridium coatings fabricated by atomic layer deposition (ALD, black) and magnetron sputtering (MS, red) compared to commercially available protected Ag (blue) and Au (green) mirror coatings from 200 nm to 20  $\mu\text{m}$  wavelength. In the inset at 20  $\mu\text{m}$  wavelength, the calculated Ir reflectivity (rhombus) is plotted using electrical resistivity according to the Hagen-Rubens relation. (b) X-ray diffraction (XRD) pattern of Ir ALD and Ir MS coatings deposited on fused silica (FS) with reference diffraction peaks shown as blue bars indicated according to Laue [42,43].

In the IR spectral range, the Ir ALD coating is higher reflective than Ir MS. The reflectance differences amount to 0.3 - 2.5% between 750 nm and 20  $\mu\text{m}$  wavelength, as the inset of Fig. 1(a) illustrates. In the VIS spectral range, the reflectance of both Ir coatings is equal within the measurement accuracy. On the other hand, Ir MS is higher reflective than the Ir ALD coating in the UV spectral range. However, the surface roughness values of 2.2 nm rms and 0.9 nm rms for Ir ALD and Ir MS, respectively, cannot fully explain these reflectance differences. In order to understand these differences, related structural properties of the Ir coatings were analyzed, as listed in Table 1 and discussed in the following paragraphs.

**Table 1. Layer properties of Ir coatings fabricated by ALD and MS.<sup>a</sup>**

Ir Layer Properties	Ir ALD	Ir MS
Surface Roughness $\sigma$ (nm rms)	$2.2 \pm 0.2$	$0.9 \pm 0.1$
Layer Thickness $d$ (nm)	$66.1 \pm 1.0$	$77.8 \pm 2.0$
Layer Density $\rho$ ( $\text{g}/\text{cm}^3$ )	$22.5 \pm 0.1$	$22.5 \pm 0.1$
Crystallite Size $L$ (nm)	$32 \pm 4$	$22 \pm 4$
Grain Size $D$ (nm)	18 - 45	13 - 25
Electrical Resistivity $\rho$ ( $10^{-8} \Omega\cdot\text{m}$ )	$9.1 \pm 0.6$	$19.7 \pm 1.2$

<sup>a</sup>Note: Surface roughness in root-mean-square (rms) determined by  $1 \times 1 \mu\text{m}^2$  atomic force microscopy (AFM) measurements; layer thickness and density by X-ray reflectometry (XRR); crystallite size by XRD using the Ir(111) peak and Scherrer's equation; grain size by scanning electron microscopy (SEM) images.

Smaller Ir crystallites reduce the reflectance of the Ir MS coating in the IR spectral range. Table 1 demonstrates that Ir ALD and Ir MS exhibit similar layer thickness and layer density, which equals bulk density with  $22.562(11) \text{ g/cm}^3$  [42]. Although their surface roughnesses differ (see also Supplement 1), the maximum scatter-induced reflectance losses [44] with  $< 0.15\%$  are negligible in the IR spectral range. However, by using the Ir(111) XRD peak (see also Fig. 1(b)) and Scherrer's equation, the estimated Ir crystallite sizes within the Ir layer yield about 32 nm for Ir ALD and 22 nm for Ir MS. Top-view SEM images of the Ir grains confirm this significant size deviation (see also Supplement 1). Thus, the significantly smaller Ir MS crystallites/grains result in more grain boundaries, which increase the electrical resistivity (or decrease the conductivity) of the Ir layer. According to Hagen & Rugens [45], the reflectivity of good conductors decreases with decreasing conductivity in the far IR (FIR) spectral range. Consequently, the calculated Ir reflectivity using electrical resistivity according to the Hagen-Rubens relation [46] matches the measured Ir reflectance at  $20 \mu\text{m}$  wavelength well, as the inset of Fig. 1(a) illustrates. At shorter wavelengths, surface scattering becomes more dominant [44], making Ir MS higher reflective than Ir ALD, as the Ir MS surface roughness is significantly lower in the UV-relevant spatial frequency range.

Both Ir coatings are poly-crystalline with a preferred Ir(111) orientation, as Fig. 1(b) also illustrates. Compared to a randomly orientated Ir powder sample [43], the Ir ALD and Ir MS coatings exhibit a preferred orientation of the crystallographic Ir(111) plane, as already reported [32,36,47,48]. Additionally, the Ir MS diffraction peaks are asymmetric and shifted to smaller angles indicating compressive stress. Indeed, the whole Ir MS coating is almost stress-compensated (with  $40 \pm 18 \text{ MPa}$ ) by the Cr adhesion layer with (reversed) tensile stress; the Ir layer exhibits compressive stress [19]. This compensation gradient from the Cr layer towards the Ir surface with a crystallite strain of  $\Delta d_{111}/d_{111} \lesssim 0.8\%$  could cause the asymmetric peak shift. From the Ir(111) peak, the Ir MS lattice constant is about  $0.3873 \text{ nm}$ , which deviates about  $0.9\%$  from the reference value of  $a = 0.38392(6) \text{ nm}$  [42]. Using this reference value, Ir ALD matches the reference diffraction peaks within the measurement uncertainty. The Ir diffraction pattern on Si wafers and FS substrates are almost identical. In Fig. 1(b), the broad peaks at  $14 - 30^\circ$  originate from the FS short-range crystalline order. From the Cr adhesion layer of Ir MS, a weakly pronounced Cr(110) peak appears at about  $44.5^\circ$ .

The Ir MS coating is smoother than Ir ALD in all IR, VIS, and UV relevant spatial frequencies ranges. In order to analyze the topography of the Ir coatings in detail, their surface roughness was investigated in a broad spectrum of spatial frequencies. The results are illustrated in Fig. 2(a), showing the Master-PSD functions of Ir ALD and Ir MS. Besides, the spatial frequency ranges relevant for light scattering (at angles of scattering from  $2 - 85^\circ$ ) in the IR, VIS, and UV spectral ranges are indicated. As already shown in Table 1, the Ir MS coating exhibits a lower surface roughness compared to Ir ALD, but also in the whole investigated spectrum of spatial frequencies. These roughness differences of the Ir layers are clearly visible as plateaux between  $0.5 \mu\text{m}^{-1}$  and  $20 \mu\text{m}^{-1}$ . Although identical double side polished Si wafers were used, these substrates also show some deviations for  $f \lesssim 0.1 \mu\text{m}^{-1}$ . Both Si wafer sides are probably polished differently, which does not affect the Ir layer roughness but should be considered for IR applications. Independently, no significant reflectance differences from  $200 \text{ nm}$  to  $20 \mu\text{m}$  wavelength were observed between multiple Ir ALD or Ir MS coatings deposited on Si wafers and FS.

Both Ir ALD and Ir MS coatings follow the roughening power-law  $\sigma(d) \sim d^\beta$  [49]. The Ir coatings were deposited using two different vacuum deposition methods: ALD as chemical vapor deposition (CVD) and MS as physical vapor deposition (PVD) technique. Therefore, additional thinner Ir coatings were investigated to check whether differences in intrinsic roughening arise during the Ir thickness growth. Figure 2(b) shows their surface roughness evolution for  $1 \times 1 \mu\text{m}^2$  and  $10 \times 10 \mu\text{m}^2$  AFM measurement areas with the Ir layer thickness. For Ir MS, surface roughening is well below the random deposition limit of  $\beta = 0.5$ , meaning diffusion processes

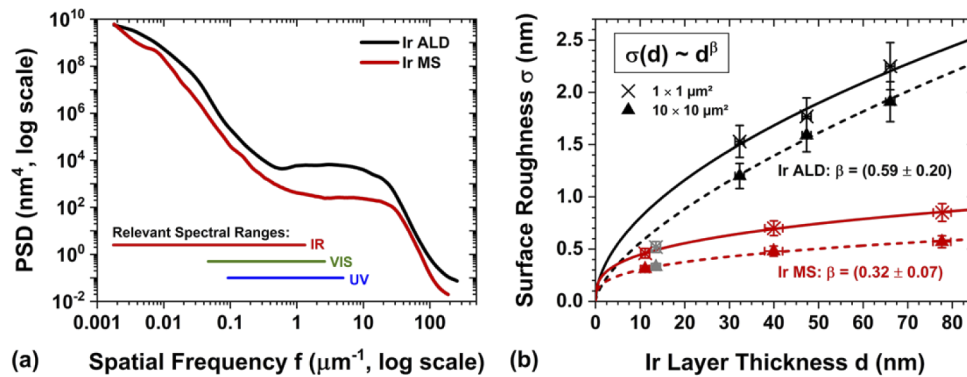


**Fig. 2.** (a) Power spectral density (PSD) functions of Ir ALD (black) and Ir MS (red) coatings determined by white light interferometry (WLI) and AFM measurements. The spatial frequency ranges relevant for light scattering in the infrared (IR), visible (VIS), and ultraviolet (UV) spectral ranges are indicated. (b) Intrinsic surface roughness evolution with the Ir layer thickness of Ir ALD and Ir MS. Both Ir coatings follow the roughening power-law for AFM  $1 \times 1 \mu\text{m}^2$  and  $10 \times 10 \mu\text{m}^2$  measurement areas.

along the growing surface smooth the Ir layer [50] due to the high-energy sputtered atoms [51]. In contrast, Ir ALD accumulates a significantly higher surface roughness with a scaling exponent of  $\beta \approx 0.59$ , probably because the  $\text{Ir}(\text{acac})_3$  precursor is chemisorbed to the surface [16] and cannot overcome the step edge barriers [50]. However, very thin Ir ALD coatings (gray symbols) exhibit a clearly lower surface roughness  $\sigma \lesssim 0.5$  nm, comparable to Ir MS. Hence, this model cannot fully describe this Ir ALD process. Premkumar et al. demonstrated that no roughening ( $\beta \approx 0$ ) occurs for thin  $\text{Al}_2\text{O}_3$  ALD coatings at all [52]. Nevertheless, the roughness evolution of Ir coatings, and metallic ALD coatings in general, has not been investigated yet.

The optical constants, meaning the refractive index  $n$  and extinction coefficient  $k$ , of the Ir coatings were evaluated by multi-experiments. For this purpose, SP, FTIR, and SE measurements were combined to cover the wavelength range from 200 nm to 20  $\mu\text{m}$ . By using the software package SpectraRay/4, a simple two-layer model was applied. The optically thick Ir layer serves as a semi-infinite substrate using a Drude-Lorentz model with five Lorentz oscillators. The Ir surface roughness is represented by an effective-medium-approximation (EMA) top layer, according to the Bruggeman approach. This EMA layer consists of 50% voids and 50% Ir; the thickness was fixed and equals the AFM ( $1 \times 1 \mu\text{m}^2$ ) surface roughness. Only the  $(2 + 2 + 3 \times 5 = 19)$  Drude-Lorentz parameters were fitted (see also Supplement 1 [53,54]). Notably, both the individual measurements and their combination provide consistent optical constants with mean-squared-error (MSE) values below 0.30. The experimental and fitted data for Ir MS are presented in Supplement 1.

In the IR spectral range, the optical constants of the Ir ALD and Ir MS coatings differ significantly. The evaluated refractive index  $n$  and extinction coefficient  $k$  of the Ir coatings are shown in Fig. 3, listed in Supplement 1, and publicly available under [55]. Additionally, reference values of Yan & Woollam [56] are displayed, which were also determined for magnetron sputtered Ir coatings. In the UV-VIS spectral range up to 750 nm wavelength, the optical constants of Ir ALD and Ir MS fit well with each other and the reference values. The absolute and relative deviations in optical constants are less than about 0.13 and 8.1%, respectively. Especially in the UV spectral range, reflectance differences caused by their surface roughness are considered in the optical constants model. However, in the IR spectral range, the optical constants of the ALD and MS deposited Ir coatings differ significantly from each other, as already observed in the reflectance spectra and explained by their different microstructure. From 750 nm to 20  $\mu\text{m}$

wavelength, the absolute and relative deviations enlarge to about 5.3 and 34% for  $n$ , and 18.9 and 32% for  $k$ , respectively. Nevertheless, the Ir MS values fit well with the reference values in the whole spectral range.

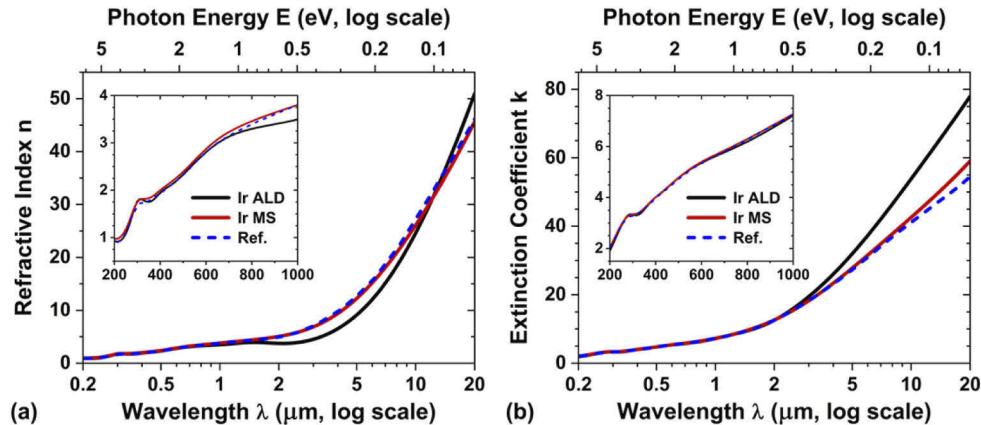


**Fig. 3.** (a) Evaluated refractive index and (b) extinction coefficient of Ir coatings fabricated by ALD (black) and MS (red) from 200 nm to 20  $\mu\text{m}$  wavelength. Especially in the IR spectral range, the optical constants differ significantly from each other. Nevertheless, the Ir MS values fit well with the reference values (Ref.) of Yan & Woollam (dashed blue) [56], which were also determined for magnetron sputtered Ir coatings.

The evaluated optical constants of Ir ALD and Ir MS complement the existing literature. The best-known optical constants originate from Lynch & Hunter [57] in Palik's *Handbook of Optical Constants of Solids* [58], analyzing studies of Weaver et al. [59] and Henke et al. [60]. However, combined with other studies by Hass et al. [61], Windt et al. [62], Kohli et al. [48], Graessle et al. [63], and Pfister et al. [64], the data differ significantly from each other. Optical constants have been evaluated using different sample forms (bulk crystals or thin films), deposition methods (evaporation or sputtering), characterization techniques (calorimetric, reflectometry, or spectroscopic ellipsometry), measurement conditions (under vacuum or ambient conditions), optical models, etc. In 2002, Yan & Woollam [56] provided valid optical constants for magnetron sputtered Ir from 140 nm to 35  $\mu\text{m}$  wavelength. Our study confirms the data of Yan & Woollam and provides additional optical constants for atomic layer deposited Ir from 200 nm to 20  $\mu\text{m}$  wavelength.

### 3.2. Stability of iridium, silver, and gold coatings

For the unprotected iridium and protected Ag and Au mirror coatings, their environmental and thermal stability was tested. Table 2 lists the environmental durability tests referring to ISO 9211-3 and related testing standards [41], thermal stability tests up to 600  $^{\circ}\text{C}$ , and their qualitative results. Regarding environmental durability, the tests correspond to the category of use C. This category C refers to applications of optical coatings under normal outdoor ambient conditions and cleaning without severe abrasion and scratching. However, the tests concerning adhesion (step 1.2 and 10.2), abrasion (step 2.2), and water solubility (step 8.2) were intensified. Acetone ( $\text{CH}_3\text{COCH}_3$ ) and ethanol ( $\text{C}_2\text{H}_5\text{OH}$ ) were used sequentially as solvents. The tests consisted of four independent test sequences: abrasion and solvent solubility (#1), climate stability (#2), and  $\text{H}_2\text{O}$  solubility (#3) for environmental durability as well as thermal stability (#4). For each of the four test sequences, one sample was used. The tests were performed one after the other according to the steps in Table 2.

Table 2. Qualitative results of environmental durability and thermal stability tests for Ir ALD, Ir MS, Ag, and Au mirror coatings.<sup>a</sup>

Step	Test	Short Description	ISO-Norm	Ir ALD				Ir MS				Ag				Au			
				#1	#2	#3	#4	#1	#2	#3	#4	#1	#2	#3	#4	#1	#2	#3	#4
1.1	Adhesion	Tape test with quick tape removal	9211-4-02-02	-	✓	✓	-	-	✓	✓	-	-	✓	✓	-	-	✓	✓	-
1.2	Adhesion	Tape test with snap tape removal	9211-4-02-03	-	✓	✓	-	-	✓	✓	-	-	✓	✓	-	-	✓	✓	-
2.1	Abrasion	100 strokes with cheesecloth, 5 N	9211-4-01-02	✓	-	-	-	✓	-	-	-	-	✓	-	-	-	-	-	-
2.2	Adhesion	40 strokes with eraser, 10 N	9211-4-01-04	✓	-	-	-	✓	-	-	-	-	✓	-	-	-	-	-	-
3	Solvents Solubility	Acetone and ethanol baths for 5 min each	9022-12-87-01	✓	-	-	-	✓	-	-	-	-	✓	-	-	-	-	-	-
4	Cold	-35 °C for 16 h	9022-2-10-07	-	✓	✓	-	-	✓	✓	-	-	✓	✓	-	-	✓	✓	-
5	Dry Heat	70 °C and < 40% RH for 6 h	9022-2-11-05	-	✓	✓	-	-	✓	✓	-	-	✓	✓	-	-	✓	✓	-
6	Damp Heat	55 °C and 92% RH for 16 h	9022-2-12-07	-	✓	✓	-	-	✓	✓	-	-	✓	✓	-	-	✓	✓	-
7	Slow Temp. Change	5x from -35 °C to 63 °C for 42 h	9022-2-14-05-1	-	✓	✓	-	-	✓	✓	-	-	✓	✓	-	-	✓	✓	-
8.1	Water Solubility	Bath in DI H <sub>2</sub> O at RT for 6 h	9211-4-04-01	-	-	✓	-	-	-	-	-	-	✓	-	-	-	-	-	✓
8.2	Water Solubility	Boiling in DI H <sub>2</sub> O for 5 min	9211-4-04-07	-	-	✓	-	-	-	-	-	-	✓	-	-	-	-	-	✓
9.1	Thermal Stability	200 °C for 24 h under vacuum	-	-	-	-	✓	-	-	-	-	-	✓	-	-	-	-	-	✓
9.2	Thermal Stability	400 °C for 24 h under vacuum	-	-	-	-	✓	-	-	-	-	-	✓	-	-	-	-	-	✓
9.3	Thermal Stability	600 °C for 24 h under vacuum	-	-	-	-	✓	-	-	-	-	-	✓	-	-	-	-	-	✓
10.1	Adhesion	Tape test with quick tape removal	9211-4-02-02	✓	✓	✓	✓	✓	✓	✓	✓	✓	✓	✓	✓	✓	✓	✓	✓
10.2	Adhesion	Tape test with snap tape removal	9211-4-02-03	✓	✓	✓	✓	✓	✓	✓	✓	✓	✓	✓	✓	✓	✓	✓	✓

<sup>a</sup>Note: The environmental durability tests were performed referring to ISO 9211-3 and related testing standards [41]. For thermal stability tests, the samples were heated at 10 K/min and passively cooled to 60 °C maximum. One sample was used for each of the four independent test sequences, whereby ✓ stands for test passed, ✗ for test failed, and - for not tested. The tests were performed one after the other according to the steps in this table.



Mirror coatings of Ir ALD, Ir MS, and Au provide stable reflectance after the abrasion and solvents solubility test sequence (#1). Figure 4 shows the reflectance after abrasion with 100 strokes cheesecloth (force of 5 N), 40 strokes eraser (10 N), and immersion baths with acetone and ethanol (5 min each). Note that abrasions after the eraser test were carefully removed from the surface with surfactants and DI H<sub>2</sub>O. Compared to untested coatings, only Ag displays minor reflectance changes in the IR spectral range from 750 nm to 20 μm, as the insets of Fig. 4 illustrate. At about 4.27 μm (= 2343 cm<sup>-1</sup>), the outliers originate from asymmetric O = C=O carbon dioxide stretching vibrations [13]. The reflectance changes of the Ir ALD, Ir MS, and Au coatings remain within the measurement uncertainties. However, visual and microscope inspection reveals fine scratches after the abrasion tests.

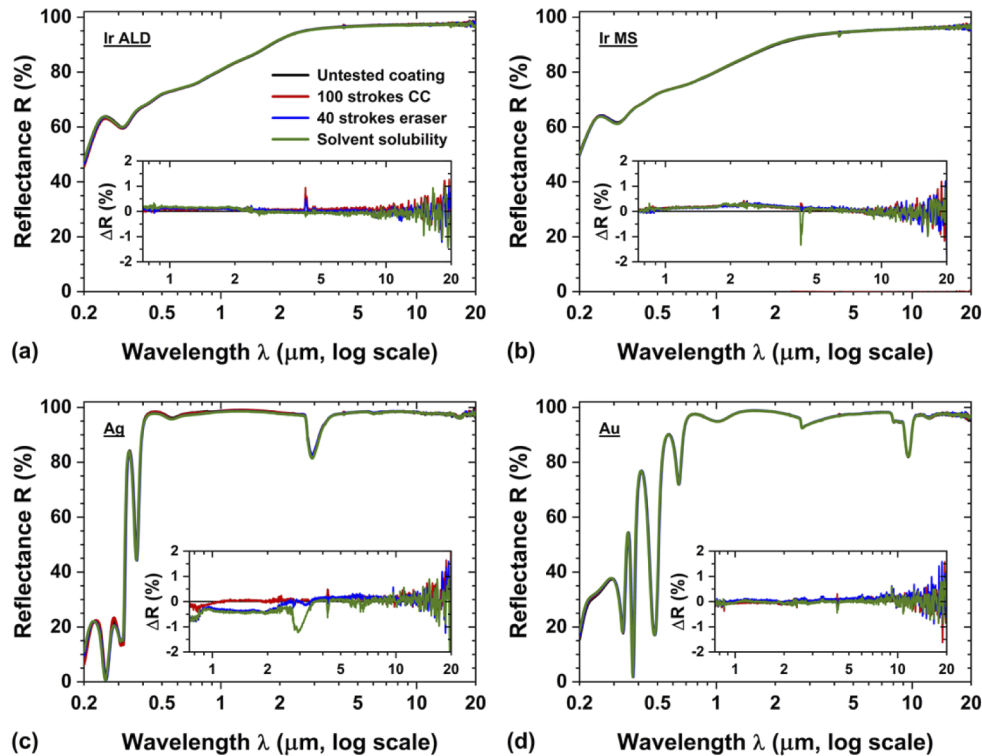


**Fig. 4.** Specular reflectance of unprotected (a) Ir ALD and (b) Ir MS coatings, and protected (c) Ag and (d) Au mirror coatings after abrasion and solvent solubility tests. The insets illustrate the reflectance changes after 100 strokes with cheesecloth (CC, red), 40 strokes with eraser (blue), and immersion baths with acetone and ethanol (green) compared to the untested coating (black).

All mirror coatings reveal surface damages after the abrasion tests, as Fig. 5 illustrates. After abrasion with 100 strokes cheesecloth, the protected Ag coating already shows fine scratches and slight greenish discoloration. After 40 strokes with an eraser (samples were rotated by about 90°), the unprotected Ir and protected Au coatings also show fine scratches on the surface. However, these scratches are not reproduced in their reflectance spectra. Especially the fine scratches on Ir MS and Au are barely visible by the unaided eye or under the microscope. For the Ag coating, significant scratches are apparent. After the solvents solubility tests, only Ag shows slight reddish to purple discoloration along the scratches. Nevertheless, all mirror coatings passed the final adhesion tests of test sequence #1. The coatings were adhesive after a single tape test with quick

tape removal and the following tape test with snap tape removal, with all tests performed on the same sample area.

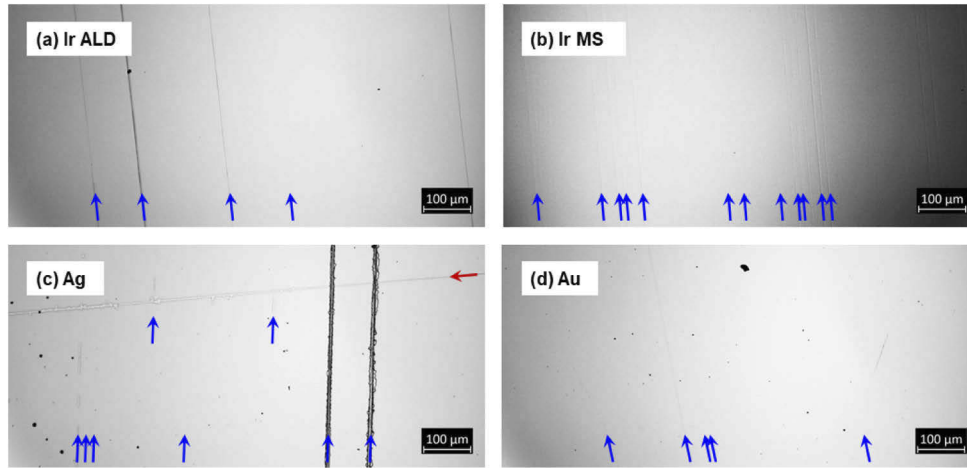


**Fig. 5.** Microscope images (top-view) of unprotected (a) Ir ALD and (b) Ir MS coatings, and protected (c) Ag and (d) Au mirror coatings after abrasion and solvent solubility tests. Arrows indicate scratches after abrasion with 100 strokes cheesecloth (red) and 40 strokes eraser (blue). Ir MS and Au display only fine scratches; Ag apparent damages.

Mirror coatings of Ir ALD, Ir MS, and Au passed the test sequences regarding climate stability (#2) and H<sub>2</sub>O solubility (#3). The climate stability tests consisted of cold (−35 °C for 16 h), dry heat (70 °C and < 40% RH for 6 h), damp heat (55 °C and 92% RH for 16 h), and slow temperature changes (5x from −35 °C to 63 °C for 42 h). For H<sub>2</sub>O solubility, the samples were immersed in DI H<sub>2</sub>O at 22 °C for 6 h and boiled in DI H<sub>2</sub>O for 5 min. Before and after these tests, adhesion tests were performed. As a result, the Ir and Au coatings show no visible physical coating defects, meaning no delamination, layer cracks, blistering, or other damages after each test. Hence, these coatings passed the environmental durability tests referring to ISO 9211-3 and the category of use C.

Protected Ag mirror coatings failed the environmental durability tests. The Ag coatings passed the climate stability and H<sub>2</sub>O solubility tests showing no visible physical coating defects. However, the coatings failed the final adhesion tests, as [Supplement 1](#) illustrates. Regarding the climate stability tests, delamination of the protective layers and reddish discoloration were visible after the second tape test with snap tape removal. Following the H<sub>2</sub>O solubility tests, delamination and reddish-purple discoloration were already visible after the first tape test with quick tape removal. Overall, the Ag protective layers seem to be relatively soft and partly water-sensitive, so abrasion and H<sub>2</sub>O can damage the coating. Thus, the damaged protective layer provides vulnerable areas for further degradation of the sensitive Ag layer reducing their reflectance over time. Still, there is continuous research on improving the Ag layer [65] and its protective coatings [66].

Coatings of unprotected Ir and protected Ag and Au are partially higher reflective after annealing at 200 °C. Finally, thermal stability and subsequent adhesion tests (#4) were performed on the Ir, Ag, and Au mirror coatings, with their qualitative results also listed in [Table 2](#). [Figure 6](#) shows the reflectance of the mirror coatings after sequential annealing for 24 h at 200 °C, 400 °C, and 600 °C under vacuum compared to the untested coating. After annealing at 200 °C, all coatings show no significant negative reflectance changes in the IR spectral range. Even on the contrary, the Ir ALD and Ir MS coatings become 0.7 - 3.7% and 0.5 - 1.5% higher reflective, respectively, in the UV spectral range. AFM and XRD on Ir ALD after annealing at 600 °C

indicate that a finer topography ( $\sigma = 2.2 \text{ nm rms} \xrightarrow{600^\circ\text{C}} 2.1 \text{ nm rms}$ ), larger Ir crystallites ( $L = 32 \text{ nm} \xrightarrow{600^\circ\text{C}} 41 \text{ nm}$ ), and consequently, fewer grain boundaries, as well as the removal of surface impurities, could cause this enhanced reflectance. For the protected Ag and Au coatings, changes of the protective layers also cause a slight reflectance increase at about  $2.9 \mu\text{m}$  and  $1.0 \mu\text{m}$ , respectively, and reflectance changes at the interference oscillations in the UV-VIS spectral range. The annealing probably reduces defects and dangling bonds in the dielectric protective layers without affecting the highly reflective metal layers [67,68].

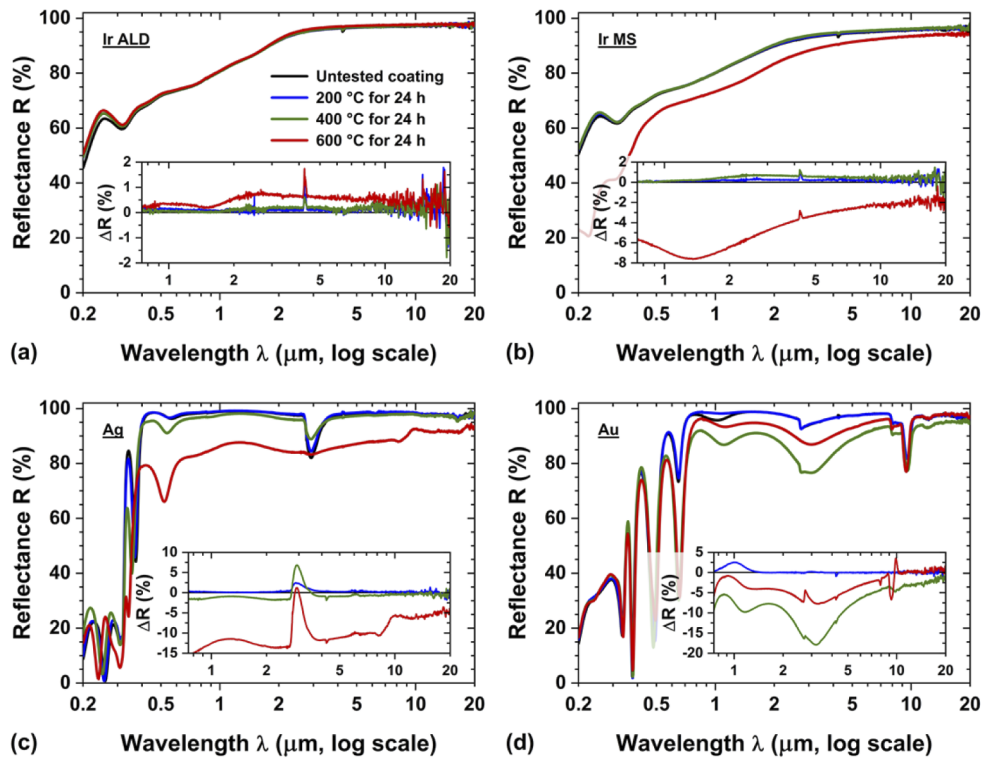


**Fig. 6.** Specular reflectance of unprotected (a) Ir ALD and (b) Ir MS coatings, and protected (c) Ag and (d) Au mirror coatings after thermal stability tests. The insets illustrate the reflectance changes after annealing for 24 h at 200 °C (blue), 400 °C (green), and 600 °C (red) compared to the untested coating (black).

After annealing at 400 °C, the Ir coatings exhibit no further significant reflectance changes. However, the protected Ag and Au coatings show reflectance losses up to 1.8% and 17.9%, respectively, in the IR spectral range. For the Ag coating, the surface appears milky and slightly cracked due to agglomeration of the Ag layer [69,70]; yellow-greenish discolored for Au.

After annealing at 600 °C, Ir ALD deposited on Si wafers retains a high reflectance with minor reflectance enhancements in the UV and IR spectral ranges. Nevertheless, the Ir ALD coating on FS displays a milky surface, resulting in diffuse scattering and specular reflectance losses of 0.5 - 2.2% between 200 nm and  $1.2 \mu\text{m}$  (see also [Supplement 1](#)). The Ir MS reflectance on both Si wafers and FS decreases by 7.6% in the IR spectral range after annealing at 600 °C compared to the unannealed coating. XRD analysis indicates an intermixing of the Ir and Cr adhesion layer. Thus, only the Ir ALD coating deposited on Si wafers is thermally stable at 600 °C. Expectably, the Ag reflectance decreases further to 82.8 - 94.5% in the IR spectral range, with their surface appearing matt, clearly cracked, and reddish discolored. Interestingly, the reflectance of the

Au coating increases again to 86.9 - 98.0% from 750 nm to 20  $\mu\text{m}$  wavelength. All Ir and Au mirror coatings passed the final adhesion tests of test sequence #4. Only the Ag protective layers delaminated after the first tape test with quick tape removal resulting in greenish discoloration.

#### 4. Conclusion

To conclude, the reflectance of unprotected iridium coatings in the MIR spectral range is comparable to typical reflectances of protected Ag and Au mirror coatings. In contrast to Ag and Au, the Ir coatings do not require protective layers, which partially diminish their reflectivity due to absorption bands in the IR spectral range. At oblique angles of incidence, the absorbing protective layers of Ag and Au will further reduce their reflectance. The Ir MS coating is environmentally durable, referring to ISO 9211-3 under normal outdoor ambient conditions and cleaning. Additionally, Ir ALD is thermally stable up to 600  $^{\circ}\text{C}$  providing a nearly constant reflectance from 200 nm to 20  $\mu\text{m}$  wavelength. These Ir coatings consisting of a substrate, one adhesion layer, and an optically thick Ir layer without protective layers are relatively easy to fabricate. Protected Ag and Au coatings are much more complex in structure, and their protective layers must be adapted for individual spectral ranges. Especially these protected mirror coatings with numerous adhesion, buffer, and protective layers are a well-kept secret of the manufacturers. Thus, these highly reflective and stable Ir mirror coatings can be easily applied as optical elements for the MIR and FIR spectral range. Using ALD, conformal Ir coatings are also possible on complex shaped or nanostructured substrates. Although protected Ag mirrors offer a higher reflectance, they are still sensitive to environmental influences. The protected Au mirrors provide high environmental stability and, thus, are preferable to the protected Ag mirrors [11] but less reflective than Ir ALD. Future research might also investigate the emissivity and resistance concerning saltwater, salt mist, or irradiation with protons and electrons of Ir coatings. However, the reflectance and, consequently, the optical constants of Ir ALD and Ir MS differ significantly due to their slightly different topography and microstructure. These differences are also evident in their surface roughness evolution, which was studied for Ir coatings for the first time. By using multi-experiments, the optical constants were evaluated using a Drude-Lorentz model, taking into account the Ir surface roughness with an EMA layer. This work publicly provides optical constants for magnetron sputtered and additionally atomic layer deposited Ir from 200 nm to 20  $\mu\text{m}$  wavelength complementing the existing literature. In combination with their PSD, this offers a comprehensive dataset to the optical community for various applications in the infrared spectral range.

**Funding.** Fraunhofer Society Attract Project (066-601020); Fraunhofer IOF Center of Excellence in Photonics; Thüringer Aufbaubank; Deutsche Forschungsgemeinschaft; Open Access Publication Fund (433052568); CRC/SFB 1375 “NOA - Nonlinear Optics down to Atomic scales” (398816777).

**Acknowledgments.** The authors thank David Kästner for technical support, Pallabi Paul for some tape tests, Michaela Mensing for some FTIR measurements, Florian Scheinpflug for support with the water solubility tests, and Thomas Müller for support with the thermal stability tests. We also thank the reviewers for their constructive comments to improve this paper. Paul Schmitt thanks the Thüringer Aufbaubank (TAB) for promoting his doctoral research studies. We acknowledge support by the Deutsche Forschungsgemeinschaft (DFG, German Research Foundation), Open Access Publication Fund of the Thüringer Universitäts- und Landesbibliothek Jena, and the DFG Collaborative Research Center (CRC/SFB) 1375 “NOA - Nonlinear Optics down to Atomic scales”.

**Disclosures.** The authors declare no conflicts of interest.

**Data availability.** The optical constants of iridium fabricated by atomic layer deposition and magnetron sputtering presented in this paper are publicly available under [www.refractiveindex.info](http://www.refractiveindex.info) [55]. Other data underlying the results presented in this paper are not publicly available but may be obtained from the authors upon reasonable request.

**Supplemental document.** See [Supplement 1](#) for supporting content.

## References

1. D. Garoli, L. V. Rodriguez De Marcos, J. I. Larruquert, A. J. Corso, R. Proietti Zaccaria, and M. G. Pelizzo, "Mirrors for space telescopes: degradation issues," *Appl. Sci.* **10**(21), 7538 (2020).
2. R. A. Keski-Kuha, C. W. Bowers, M. A. Quijada, J. B. Heaney, B. Gallagher, A. McKay, and I. Stevenson, "James Webb Space Telescope optical telescope element mirror coatings," *Proc. SPIE* **8442**, 84422J–12 (2012).
3. V. Cotroneo, R. Bruni, T. Döhring, D. Ferreira, E. Gibertini, P. Henriksen, L. Magagnin, S. Massahi, G. Pareschi, S. Romaine, L. Sethares, G. Sironi, D. Spiga, G. Tagliaferri, and G. Valsecchi, "Development of low-density coatings for soft x-ray reflectivity enhancement for ATHENA and other missions," *Proc. SPIE* **11852**, 169 (2021).
4. R. Dasbach, Temperature- and corrosion-stable surface reflector, US 10436955 B2.
5. G. Hass, J. B. Heaney, H. Herzig, J. F. Osantowski, and J. J. Triolo, "Reflectance and durability of Ag mirrors coated with thin layers of Al<sub>2</sub>O<sub>3</sub> plus reactively deposited silicon oxide," *Appl. Opt.* **14**(11), 2639–2644 (1975).
6. J. Pivot, "Mechanical properties of SiOx thin films," *Thin Solid Films* **89**(2), 175–190 (1982).
7. S. Schwinde, M. Schürmann, R. Schlegel, J. Kinast, R. J. Dorn, J. L. Lizon, S. Tordo, and N. Kaiser, "Protected silver coatings for reflectors," *CEAS Space J* **11**(4), 579–587 (2019).
8. M. Boccas, T. Vucina, C. Araya, E. Vera, and C. Ahhee, "Protected-silver coatings for the 8-m Gemini telescope mirrors," *Thin Solid Films* **502**(1-2), 275–280 (2006).
9. F. Anjum, D. M. Fryauf, R. Ahmad, A. C. Phillips, and N. P. Kobayashi, "Improving silver mirrors with aluminum oxynitride protection layers: variation in refractive index with controlled oxygen content by radiofrequency magnetron sputtering," *J. Astron. Telesc. Instrum. Syst.* **4**(04), 1–10 (2018).
10. S. Schwinde, M. Schürmann, N. Kaiser, and T. Tünnermann, "Investigation of SiO<sub>2</sub>-Al<sub>2</sub>O<sub>3</sub> nanolaminates for protection of silver reflectors," *Appl. Opt.* **56**(4), C41–C46 (2017).
11. S. Schwinde, S. Shestaeva, S. Stempfhuber, H. von Lukowicz, J. Kuhnhehn, and S. Schröder, "Au coatings for space based reflectors," *Proc. SPIE* **11852**, 62 (2021).
12. N. T. McDevitt and W. L. Baun, "Infrared absorption study of metal oxides in the low frequency region (700–240 cm<sup>-1</sup>)," *Spectrochim. Acta* **20**(5), 799–808 (1964).
13. V. P. Tolstoy, I. Chernyshova, and V. A. Skryshevsky, *Handbook of Infrared Spectroscopy of Ultrathin Films* (John Wiley & Sons, 2003).
14. H. Herzig, A. R. Toft, and C. M. Fleetwood, "Long-duration orbital effects on optical coating materials," *Appl. Opt.* **32**(10), 1798–1804 (1993).
15. W.-P. Wu and Z.-F. Chen, "Iridium coating: processes, properties and application. Part I," *Johnson Matthey Technol. Rev.* **61**(1), 16–28 (2017).
16. L. Ghazaryan, K. Pfeiffer, P. Schmitt, V. Beladiya, S. Kund, and A. Szeghalmi, "Atomic Layer Deposition," in *digital Encyclopedia of Applied Physics* (Wiley-VCH Verlag, 2020), pp. 1–44.
17. J. Vila-Comamala, S. Gorelick, E. Färm, C. M. Kewish, A. Diaz, R. Barrett, V. A. Guzenko, M. Ritala, and C. David, "Ultra-high resolution zone-doubled diffractive X-ray optics for the multi-keV regime," *Opt. Express* **19**(1), 175–184 (2011).
18. A.-C. Probst, T. Döhring, M. Stollenwerk, M. Wen, and L. Proserpio, "Iridium coatings for space based x-ray optics," *Proc. SPIE* **10562**, 177 (2017).
19. A.-C. Probst, T. Begou, T. Döhring, S. Zeising, M. Stollenwerk, J. Stadtmüller, F. Emmerich, and J. Lumeau, "Coating stress analysis and compensation for iridium-based x-ray mirrors," *Appl. Opt.* **57**(29), 8775–8779 (2018).
20. M. C. Weisskopf, "Chandra x-ray optics," *Opt. Eng.* **51**(1), 011013 (2012).
21. J. I. Larruquert, J. A. Mendez, and J. A. Aznarez, "Non-oxidized Al-overcoated Ir bilayers with high reflectance in the extreme ultraviolet above 50 nm," *Opt. Eng.* **41**(6), 1418–1424 (2002).
22. P. L. Henriksen, D. D. M. Ferreira, S. Massahi, M. C. Civitani, S. Basso, J. Vogel, J. R. Armendariz, E. B. Knudsen, I. G. Irastorza, and F. E. Christensen, "Iridium thin-film coatings for the BabyIAXO hybrid X-ray optic," *Appl. Opt.* **60**(22), 6671–6681 (2021).
23. T. Weber, T. Käsebier, A. Szeghalmi, M. Knez, E.-B. Kley, and A. Tünnermann, "Iridium wire grid polarizer fabricated using atomic layer deposition," *Nanoscale Res. Lett.* **6**(1), 558 (2011).
24. D. Briand, B. van der Schoot, N. F. de Rooij, H. Sundgren, and I. Lundstrom, "A low-power micromachined MOSFET gas sensor," *J. Microelectromech. Syst.* **9**(3), 303–308 (2000).
25. E. N. E. Sawy and V. I. Birss, "Nano-porous iridium and iridium oxide thin films formed by high efficiency electrodeposition," *J. Mater. Chem.* **19**(43), 8244–8252 (2009).
26. M. Stollenwerk, T. Schäfer, J. Stadtmüller, T. Döhring, D. Freudenmann, and N. Röcke, "Sputtered highly effective iridium catalysts: a new approach for green satellite propulsion," *J. Mater. Sci.* **56**(16), 9974–9984 (2021).
27. M. Franz, R. Junghans, P. Schmitt, A. Szeghalmi, and S. E. Schulz, "Wafer-level integration of self-aligned high aspect ratio silicon 3D structures using the MACE method with Au, Pd, Pt, Cu, and Ir," *Beilstein J. Nanotechnol.* **11**, 1439–1449 (2020).
28. S. Shirvaliloo and H. Kangarloo, "Production of iridium metal thin films for application as electrodes in DRAMs and FRAMs," *J. Electr. Electron. Eng.* **3**(2), 35–38 (2015).
29. A. Hofer, S. Bochmann, and J. Bachmann, "Properties, performance and stability of iridium-coated water oxidation electrodes based on anodized titanium felts," *Sustainable Energy Fuels* **5**(2), 478–485 (2021).
30. R. Hemphill, M. Hurwitz, and M. G. Pelizzo, "Osmium atomic-oxygen protection by an iridium overcoat for increased extreme-ultraviolet grating efficiency," *Appl. Opt.* **42**(25), 5149–5157 (2003).

31. M. Kajiwara, S. Uemiya, T. Kojima, and E. Kikuchi, "Rhodium- and iridium-dispersed porous alumina membranes and their hydrogen permeation properties," *Catal. Today* **56**(1-3), 83–87 (2000).
32. P. Schmitt, V. Beladiya, N. Felde, P. Paul, F. Otto, T. Fritz, A. Tünnermann, and A. V. Szeghalmi, "Influence of substrate materials on nucleation and properties of iridium thin films grown by ALD," *Coatings* **11**(2), 173 (2021).
33. P. Genevée, E. Ahiavi, N. Janunts, T. Pertsch, M. Oliva, E.-B. Kley, and A. Szeghalmi, "Blistering during the atomic layer deposition of iridium," *J. Vac. Sci. Technol. A* **34**(1), 01A113 (2016).
34. H. K. Pulker, *Coatings on Glass*, 2nd ed. (Elsevier, 1999).
35. A. Büttner, A.-C. Probst, F. Emmerich, C. Damm, B. Rellinghaus, T. Döhring, and M. Stollenwerk, "Influence of sputtering pressure on microstructure and layer properties of iridium thin films," *Thin Solid Films* **662**, 41–46 (2018).
36. A.-C. Probst, M. Stollenwerk, F. Emmerich, A. Büttner, S. Zeising, J. Stadtmüller, F. Riethmüller, V. Stehlíková, M. Wen, L. Proserpio, C. Damm, B. Rellinghaus, and T. Döhring, "Influence of sputtering pressure on the nanostructure and the X-ray reflectivity of iridium coatings," *Surf. Coat. Technol.* **343**, 101–107 (2018).
37. S. Massahi, L. M. Vu, D. D. M. Ferreira, F. E. Christensen, N. Gellert, P. L. Henriksen, S. Svendsen, A. S. Jegers, M. Collon, B. Landgraf, D. Girou, A. Thete, B. Shortt, I. Ferreira, and M. Bavdaz, "Balancing of residual stress in thin film iridium by utilizing chromium as an underlayer," *Proc. SPIE* **11444**, 744–759 (2020).
38. A. Duparré, J. Ferre-Borrull, S. Glied, G. Notni, J. Steinert, and J. M. Bennett, "Surface characterization techniques for determining the root-mean-square roughness and power spectral densities of optical components," *Appl. Opt.* **41**(1), 154–171 (2002).
39. P. Scherrer, "Bestimmung der Größe und der inneren Struktur von Kolloidteilchen mittels Röntgenstrahlen," *Nachrichten von der Gesellschaft der Wissenschaften zu Göttingen, Mathematisch-Physikalische Klasse* **1918**, 98–100 (1918).
40. L. J. Swartzendruber, *Correction factor tables for four-point probe resistivity measurements on thin, circular semiconductor samples. Technical Note* (National Bureau of Standards, 1964).
41. DIN Deutsches Institut für Normung e. V., *Optik und Photonik - Optische Schichten - Teil 3: Umweltbeständigkeit (ISO 9211-3:2008)* (Beuth Verlag, 2008).
42. J. W. Arblaster, "Crystallographic Properties of Iridium," *Platinum Met. Rev.* **54**(2), 93–102 (2010).
43. H. E. Swanson and E. Tatge, *Standard X-ray Diffraction Powder Patterns* (National Bureau of Standards, 1955).
44. H. E. Bennett and J. O. Porteus, "Relation Between Surface Roughness and Specular Reflectance at Normal Incidence," *J. Opt. Soc. Am.* **51**(2), 123–129 (1961).
45. E. Hagen and H. Rubens, "Über Beziehungen des Reflexions- und Emissionsvermögens der Metalle zu ihrem elektrischen Leitvermögen," *Ann. Phys.* **316**(8), 873–901 (1903).
46. R. Gross and A. Marx, *Festkörperphysik*. (In German), 2. Auflage (De Gruyter Oldenbourg, 2014).
47. T. Aaltonen, M. Ritala, V. Sammelselg, and M. Leskelä, "Atomic layer deposition of iridium thin films," *J. Electrochem. Soc.* **151**(8), G489–G492 (2004).
48. S. Kohli, D. Niles, C. D. Rithner, and P. K. Dorhout, "Structural and optical properties of Iridium films annealed in air," *Adv. X-Ray Anal.* **45**, 352–358 (2002).
49. M. Kotrla, "Growth of rough surfaces," *Czech. J. Phys.* **42**(5), 449–477 (1992).
50. J. Krug, "Power laws in surface physics: the deep, the shallow and the useful," *Physica A* **340**(4), 647–655 (2004).
51. R. F. Bunshah, ed., *Handbook of Deposition Technologies for Films and Coatings: Science, Technology, and Applications*, 2nd Edition (Noyes Publications, 1994).
52. P. A. Premkumar, A. Delabie, L. N. J. Rodriguez, A. Moussa, and C. Adelman, "Roughness evolution during the atomic layer deposition of metal oxides," *J. Vac. Sci. Technol. A* **31**(6), 061501 (2013).
53. O. Stenzel, *Optical Coatings: Material Aspects in Theory and Practice* (Springer-Verlag, 2014).
54. J. Jaiswal, S. Mourya, G. Malik, S. Chauhan, A. Sanger, R. Daipuriya, M. Singh, and R. Chandra, "Determination of optical constants including surface characteristics of optically thick nanostructured Ti films: analyzed by spectroscopic ellipsometry," *Appl. Opt.* **55**(29), 8368–8375 (2016).
55. M. N. Polyanskiy, "Refractive index database," <https://refractiveindex.info>. Accessed on 2021-10-28.
56. L. Yan and John A. Woollam, "Optical constants and roughness study of dc magnetron sputtered iridium films," *J. Appl. Phys.* **92**(8), 4386–4392 (2002).
57. D. W. Lynch and W. R. Hunter, "Comments on the optical constants of metals and an introduction to the data for several metals," in *Handbook of Optical Constants of Solids*, E. D. Palik, ed. (Academic Press, 1985), pp. 275–367.
58. E. D. Palik, *Handbook of Optical Constants of Solids* (Academic Press, 1998).
59. J. H. Weaver, C. G. Olson, and D. W. Lynch, "Optical investigation of the electronic structure of bulk Rh and Ir," *Phys. Rev. B* **15**(8), 4115–4118 (1977).
60. B. L. Henke, P. Lee, T. J. Tanaka, R. L. Shuimabukuro, and B. K. Fujikawa, "The Atomic Scattering Factor,  $f_1 + if_2$ , for 94 Elements and for the 100 to 2000 eV photon energy region," *AIP Conf. Proc.* **75**, 340–388 (1981).
61. G. Hass, G. F. Jacobus, and W. R. Hunter, "Optical Properties of evaporated iridium in the vacuum ultraviolet from 500 Å to 2000 Å," *J. Opt. Soc. Am.* **57**(6), 758–762 (1967).
62. D. L. Windt, W. C. Cash, M. Scott, P. Arendt, B. Newnam, R. F. Fisher, and A. B. Swartzlander, "Optical constants for thin films of Ti, Zr, Nb, Mo, Ru, Rh, Pd, Ag, Hf, Ta, W, Re, Ir, Os, Pt, and Au from 24 Å to 1216 Å," *Appl. Opt.* **27**(2), 246–278 (1988).
63. D. E. Graessle, R. Soufli, A. L. Aquila, E. M. Gullikson, R. L. Blake, and A. J. Burek, "Iridium optical constants for the Chandra X-ray Observatory from reflectance measurements of 0.05–12 keV," *Proc. SPIE* **5165**, 469–481 (2004).

64. N. A. Pfister, K. A. Grossklaus, M. A. Stevens, and T. E. Vandervelde, "Effect of microstructure on the optical properties of sputtered iridium thin films," *Opt. Mater. Express* **10**(4), 1120–1128 (2020).
65. A. S. Baburin, A. I. Ivanov, E. S. Lotkov, O. S. Sorokina, I. A. Boginskaya, E. V. Sergeev, K. A. Buzaverov, T. G. Konstantinova, D. O. Moskalev, Z. Issabayeva, I. A. Ryzhikov, and I. A. Rodionov, "Epitaxial silver films morphology and optical properties evolution over two years," *Coatings* **10**(10), 911 (2020).
66. D. M. Fryauf, A. C. Phillips, and N. P. Kobayashi, "Critical processing temperature for high-performance protected silver mirrors," *J. Astron. Telesc. Instrum. Syst.* **7**(03), 1–11 (2021).
67. M. Tilsch, V. Scheuer, and T. T. Tschudi, "Effects of thermal annealing on ion-beam-sputtered SiO<sub>2</sub> and TiO<sub>2</sub> optical thin films," *Proc. SPIE* **3133**, 163–175 (1997).
68. J.-P. Masse, H. Szymanowski, O. Zabeida, A. Amassian, J. E. Klemberg-Sapieha, and L. Martinu, "Stability and effect of annealing on the optical properties of plasma-deposited Ta<sub>2</sub>O<sub>5</sub> and Nb<sub>2</sub>O<sub>5</sub> films," *Thin Solid Films* **515**(4), 1674–1682 (2006).
69. S. K. Sharma and J. Spitz, "Hillock formation, hole growth and agglomeration in thin silver films," *Thin Solid Films* **65**(3), 339–350 (1980).
70. S. Gledhill, K. Steyer, C. Weiss, and C. Hildebrandt, "HiPIMS and DC magnetron sputter-coated silver films for high-temperature durable reflectors," *Coatings* **9**(10), 593 (2019).